PHILOSOPHICAL TRANSACTIONS OF THE ROYAL SOCIETY A MATHEMATICAL, PHYSICAL & ENGINEERING SCIENCES

Magnetosphere--Ionosphere Coupling: Effects of Plasma Alfven Wave Relative Motion

P. J. Christiansen and C. T. Dum

Phil. Trans. R. Soc. Lond. A 1989 **328**, 195-207
doi: 10.1098/rsta.1989.0031

Phil. Trans. R. Soc. Lond. A **328**, 195–207 (1989)
Printed in Great Britain

Magnetosphere–ionosphere coupling: effects of plasma Alfvén wave relative motion

By P. J. Christiansen[1] and C. T. Dum[2]

[1] *Space and Plasma Physics Group, School of Mathematical and Physical Sciences, University of Sussex, Brighton BN1 9QH, U.K.*

[2] *Max-Planck-Institut für Physik und Astrophysik, Institut für extraterrestrische Physik, 8046 Garching, F.R.G.*

The introduction of relative perpendicular motion between a flux-tube supporting shear Alfvén wave activity and the background plasma is studied in the context of the coupling of a wave generating region with a distant ionosphere. The results of a representative simulation, using an extended version of the code developed by Lysak & Dum (*J. geophys. Res.* **88**, 365 (1983)), are used as a basis for interpreting some aspects of recent satellite observations.

From the magnetohydrodynamic (MHD) viewpoint, the coupling of distant regions of enhanced magnetospheric convection and the auroral ionosphere is accomplished by the propagation of shear Alfvén waves between the generating region and the low-altitude boundary. Setting up field-aligned current systems, whether a final quasi-equilibrium state exists or not, must therefore involve shear wave related dynamical processes, both initially and whenever changes occur in either the generator or in the ionosphere. Time-dependent aspects of this problem have been discussed by Scholer (1970), Maltsev *et al.* (1977), Mallinkrodt & Carlson (1978), Goertz & Boswell (1979) and Nishida (1979).

It has been known for some time that though the group velocity of shear waves is strongly aligned with the background magnetic field, the linear dispersion relation for waves with large inverse scale lengths $k_\perp$ can be considerably modified in both warm, $\beta > m_e/m_i$ (Hasegawa 1976), and cool, $\beta < m_e/m_i$ (Goertz & Boswell 1979), régimes by finite ion larmor radius and electron inertial effects respectively. The field-aligned current densities associated with such waves can be considerable and this adds a further complicating element to dynamical studies, the presence of regions of turbulent resistivity arising from instabilities driven by these currents (Mallinkrodt & Carlson 1978; Dum *et al.* 1981, 1985). In the low-β régime the currents will be carried by non-resonant background electrons (with contributions from suprathermal runaway components accelerated by parallel electric fields present in regions of turbulent friction), and it has been argued by Lysak & Hudson (1978) and Lysak & Dum (1983) that when altitude variations of the plasma parameters are taken into account, current driven instabilities are most likely to occur in relatively extended regions above about 6000 km on auroral field lines.

Introduction

The dynamics of short perpendicular-scale shear Alfvén wave propagation in extended systems has recently been studied using a straight geometry, two-fluid, two-dimensional, MHD code, by Lysak & Dum (1983) (hereafter L.D.). This simulation model contains the crucial

new element with respect to earlier studies in that a region of turbulent resistivity is introduced between the distant wave generating and the ionospheric ends of the simulation (see also Haerendel 1983; Dum 1985).

The model consists in solving Maxwell's equations and equations of motion for electrons and ions i.e. (in c.g.s. units)

$$\begin{aligned}
\partial B_y/\partial t &= -c\,(\partial E_x/\partial z - \partial E_z/\partial x),\\
J_x &= -c/4\pi\,\partial B_y/\partial z,\\
J_z &= c/4\pi\,\partial B_y/\partial x,\\
\partial n/\partial t &= 1/e\,\partial J_z/\partial z = -1/e\,\partial J_x/\partial x,\\
\partial J_z/\partial t - \partial/\partial z\,(J_z^2/ne) &= (ne^2/m_e)\,E_z - \nu^*(u_z)\,(J_z - neu_c\,\mathrm{sgn}\,J_z),\\
J_x &= nm_i c^2/eB_0^2\,[\partial/\partial t + \partial U_x/\partial x]\,E_x,
\end{aligned}$$

where low-frequency variations in x, z of the electric field E, magnetic field B, current densities J, electron and ion drift speeds $u_z = -J_z/ne$ and $U_x = J_x/ne$ respectively, are considered. The background magnetic field B_0 is in the z direction and terms of the order of the ion to electron mass ratio m_e/m_i are neglected.

In L.D. the anomalous collision frequency ν^* is assumed to obey a law of the form $\nu^* = \nu_1 + \nu_2\,[(|u_z| - u_c)/u_c]^2$ when the parallel electron drift velocity u_z exceeds the critical drift for instability appropriate to resonance broadening saturation of electrostatic ion cyclotron turbulence (Dum & Dupree 1970; L.D. Appendix B). It is justified on the grounds that the field-aligned current systems associated with shear wave propagation are, in low-β plasmas, carried by drifting, non-resonant, cool electron background whose relative motion with respect to the inert ion background can give rise at least to ion cyclotron harmonic (ICH) (and possible ion sound) (Kindel & Kennel 1971) instability over extended regions along the flux tube. In our choice of background parameters we follow Lysak & Hudson (1978) and L.D. who argue that regions above 6000 km height are especially favoured for such turbulent processes.

Simulation results

The simulation is carried out on a grid of 40×80 cells in the xz-plane, with the small x-dimension, $L_x = 34$ km, and $L_z = 26000$ km. It is bounded at the top by prescribing $B_y(x, z = 0, t)$ as a current generator, and at the bottom by setting the ionosphere as a sheet conductor with height-integrated Pedersen conductivity $\Sigma_P(x, z = L_z) = 10$ mho†. The boundary conditions on the sides of the box, in the direction perpendicular to the background magnetic field $B_0\hat{z}$ are $E_x, B_y = 0$ at $x = 0, L_x$ with symmetry $B_y(-x) = -B_y(x)$, $E_x(-x) = -E_x(x)$. For the generator configuration used here the implied constraints of zero current, $J_x = -c/4\pi\,\partial B_y/\partial x$, and wave energy flow, $S_x = -cE_z B_y/4\pi + U_x\,(c/V_A)^2\,E_x^2/8\pi$, are unimportant.

The region in which turbulent resistivity may be driven up is set, as in L.D., by prescribing a parabolic (in z) profile for the critical current, $J_c(z)$ centred at $z = 0.75L_z$, with an effective half-width of $z = \pm 0.1L_z$.

We choose the background parameters $n = 25\ \mathrm{cm}^{-3}$, $B_0\hat{z} = 0.06$ G, to be roughly appropriate to auroral field-line values at 6000 km height (Mozer *et al.* 1979; Persoon *et al.* 1984) while maintaining a reasonable separation of propagation effects between various parts

† 1 mho = 1 Ohm^{-1}.

PHILOSOPHICAL TRANSACTIONS OF THE ROYAL SOCIETY A MATHEMATICAL, PHYSICAL & ENGINEERING SCIENCES

of the system. Clearly the effect of refractive index variations due to density and $B_0\hat{z}$ variations along the auroral flux tube are not taken into account.

The simulation has been initiated by prescribing a generator boundary condition of the form

$$B_y(x, z = 0, t) = B_{y0} f_1(t) f_2(x - V_x t),$$

where $f_1(t)$ is a linear ramp which reaches a constant value at $t = 0.2$, and $f_2(x, t = 0)$ has a positive saw tooth form spanning the interval $x = (\frac{3}{8}L_x, \frac{5}{8}L_x)$, generating two uniform, opposed current sheets in z. V_x is chosen such that the pulse crosses its own full width in one time unit, the travel time of an Alfvén wave from generator to ionosphere. The pulse amplitude corresponds to a relative perturbation $B_y/B_0 = 0.2\,\%$, and the associated current density exceeds the minimum critical value for the onset of the electrostatic ion cyclotron turbulence in the resistive zone by a factor of 5 i.e. $(J_z/J_c)_{\min} = 5$ in the centre of the turbulent zone. The resistivity coefficients scaled to the ion gyrofrequency are $\nu_1/\Omega_i = 0.4$, $\nu_2/\Omega_i = 0.1$.

The three frames of figure 1 show contours of constant B_y, the shear B-field component (also current flow lines in this two-dimensional geometry), together with electric field vectors $\boldsymbol{E} = [E_x, ME_z]$, where M is a magnification of *ca.* 2000, at several times during the run.

In the first frame, figure 1*a*, recorded at $t = 0.8$, the pulse front has just reached the turbulent zone (deliniated by the hatching on the left side of the box). The oblique x–t characteristics are a result of the finite V_x value, but should strictly be viewed from the moving plasma frame, the relative motion being the result of an E_y-directed convection field. At time $t = 0.8$ the current flow is relatively uncomplicated, with downward current (carried by upgoing electrons) along the trailing flank, and vice versa for the leading edge. The related electron drift has been initiated by the transient parallel electric field $E_z(x, t)$ (Goertz & Boswell 1978) in the pulse head. Current closure is by means of ion polarization drift, (except for the ionosphere), and at this stage is across the pulse head in the region of negative $\partial B_y/\partial z$. Because of the relatively gentle time ramping of the pulse via $f_1(t)$ the parallel current density is still subcritical, and the flaring of the pulse together with the subsidiary wavelets fanning out from the trailing edge are simply linear dispersion features due to the finite value of $k_\perp c/\omega_p$ (finite electron inertia) discussed by Goertz (1981).

The Poynting flux is essentially downwards, $S_z \approx c(E_x B_y)/4\pi$, with the inertial E_z contributing to the flaring and fanning features via perpendicular flux $S_x = c(E_z B_y)/4\pi$. These latter features can be artificially suppressed by removing the inertial terms from the electron equation without significant effect on later evolution of the simulation.

In the second frame, a snapshot at $t = 1.0$, the transmitted part of the pulse has just reached the ionosphere. Reflections from the turbulent zone giving partial decoupling of the generator from the ionosphere (L.D.) can already be seen on both leading and trailing edges above the zone (S_z on the trailing edge is small but negative, i.e. up), but the most obvious effect is the resistive broadening of the current system in its passage through the turbulent zone, and the appearance of regions of up and down parallel electric fields E_z within it.

The next views are taken at $t = 1.2$ and $t = 1.4$ as the ionospherically reflected component passes back through the turbulent region and moves up towards the generator plane. The maximum value of B_y occurs at the ionosphere as a result of reflection from a highly conducting ionosphere.

The approximate doubling of the transmitted current density leads to a second build up of turbulent resistivity, a further broadening of the current system, and further increase in E_z

PHILOSOPHICAL TRANSACTIONS OF THE ROYAL SOCIETY A MATHEMATICAL, PHYSICAL & ENGINEERING SCIENCES

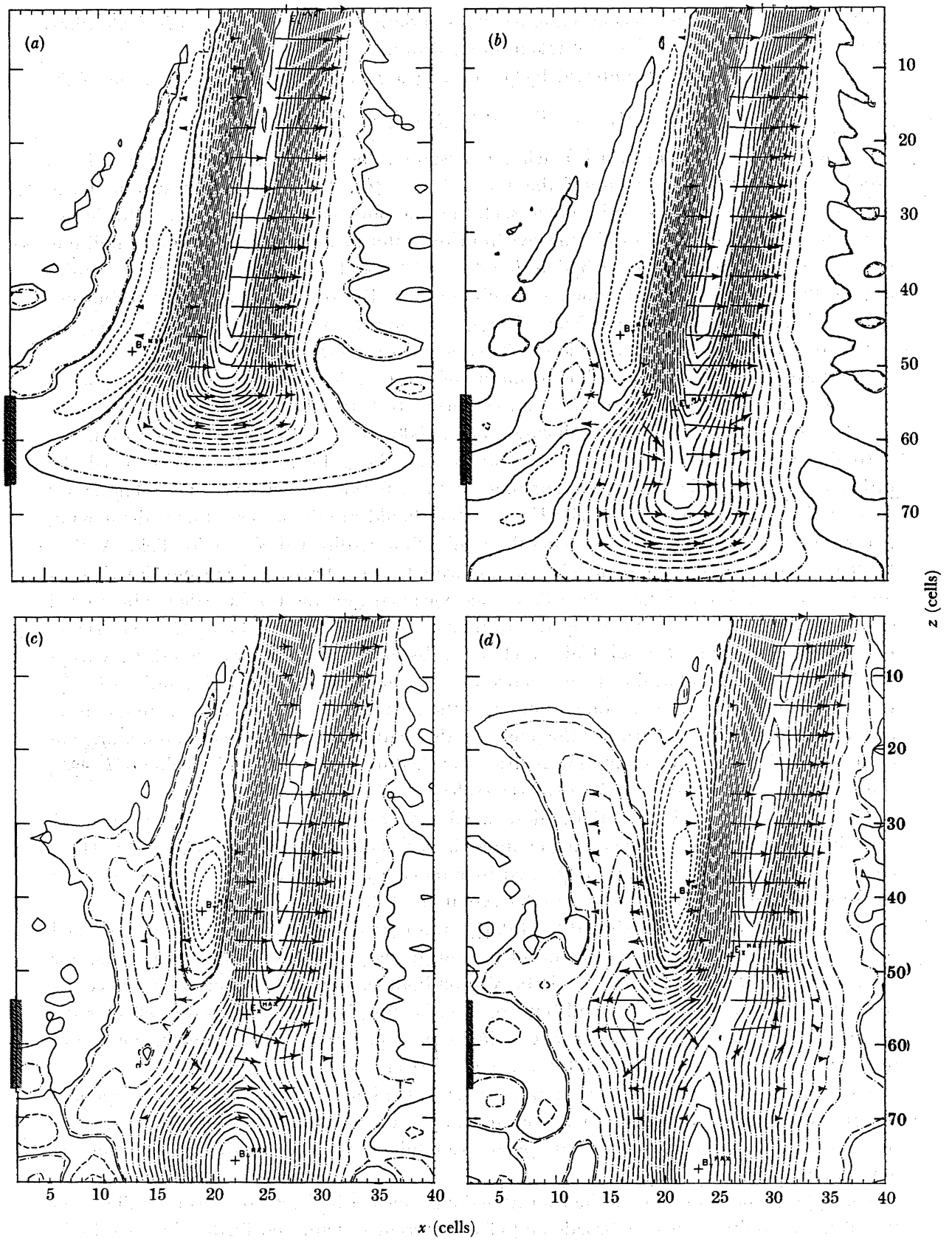

FIGURE 1. For description see opposite.

PHILOSOPHICAL TRANSACTIONS OF THE ROYAL SOCIETY A MATHEMATICAL, PHYSICAL & ENGINEERING SCIENCES

during this second pass. Above the resistive region two more, identifiably different reflection features can be seen, clarified by the relative perpendicular motion. That closest to the trailing edge shows reversed B_y features but with E_x in the same sense as the generator field, and is clearly the result of reflection from the resistive region, as reported by L.D. The second, further downstream, arises from reflections occurring a little later in time. It has reversed E_x, and B_y in the normal sense, and is the result of reflection from the refractive index transition that is experienced as the wave emerges from the bottom of the turbulent region (we recall that the refractive index N is modified by the presence of collisions such that

$$N^2 = (k_\parallel V_A/\omega)^2 = 1 + (k_\perp^2 c^2/\omega_p^2)\,[1 + i\,\nu/\omega],$$

(Lysak & Carlson 1981).

The energy flow is now more complicated, down the leading flank from the generator towards the ionosphere and being partly diverted into and dissipated in the resistive region ($S_x \neq 0$). Energy returns from the ionosphere on the trailing edge to be further partly diverted and dissipated in its upward flow, leading to a further enhancement of the parallel electric fields.

Up to this point the simulation results *vis-à-vis* behaviour in the turbulent region are independent of the top and side boundary conditions. The $t = 1.0$ plot can be taken as representing a system with a perfectly absorbing ionosphere, while that at $t = 1.4$ could be viewed as representing a system with a perfectly absorbing generator. By fixing B_y at the generator plane we have assumed an ideal constant current generator, so that at times later than $t = 1.5$, downstream of the injection region no current will be accepted. As the generator responds like a perfect current generator new features develop. This problem has been addressed by Lysak (1985) and will not be discussed further here.

FIGURE 1. Shear wave magnetic field (B_y) and electric field (E_x, ME_z) plots at several instants during the simulation. The x (horizontal), z (vertical down) coordinate system (40×80 cells) has very disparate physical dimensions with $L_x = 34.2$ km, $L_z = 26000$ km appropriate to short perpendicular scales of interest $2\pi c/L_x\omega_p = 0.1$. The background parameters $B_0 = B_0\hat{z}$ (not shown) $= 6 \times 10^3$ nT, $n_0 = 25$ cm^{-3}, $V_{A0} = 2.6 \times 10^4$ km s^{-1}, appropriate to altitudes of *ca.* $1R_E$ on auroral field lines. The generator lies in the $z = 0$ plane and the ionosphere (height-integrated conductivity $\Sigma_p = 10$ mho) in the $z = L_z$ plane. The region in which local current driven anomalous resistivity can occur is shown by the cross hatching on the right, centred at $z = 0.75L_z$ (cell 60) with a half width of $0.1L_z$. Time is measured in units of the one way travel time from generator to ionosphere ($L_z/V_{A0} = 1$ s), thus an Alfvén pulse will reach the centre of the turbulent zone at $t = 0.75$. Contours of constant B_y, (current flow lines in 2D) are coded such that for positive B_y the dashes of the dot–dash pattern increase in length with increasing B_y. Regions of negative B_y are enclosed by short dashed contours. E vectors are shown by arrows. The E_z component is for clarity magnified by a factor of *ca.* 10^3 to clarify regions of significant parallel electric fields, E_z. (*a*) $t = 0.8$. The pulse head has reached the turbulent zone, but because of the time ramping $f_1(t)$ currents ($j_z \propto \partial B_y/\partial x$) are still subcritical, and flow down the trailing flank, and up on the leading flank. The maximum values for $B_y = 20$ nT and $E_x = 0.59$ V m^{-1} are located at the cell (28,0) i.e. in the generator plane. See text for further details. (*b*) $t = 1.0$. Wave energy reaches the lower ionosphere boundary. The pulse profile is broadened as a result of its passage through the resistive region, where significant dissipation ($j \cdot E > 0$) occurs centred on cells (17,60) and (25,60), where down (up) parallel electric field $(E_z)_{max} \approx 0.8$ mV m^{-1} also exert. Reflections from the top of the turbulent region enhance E_x with $(E_x)_{max} = 0.63$ mV m^{-1} at (25,56). The region of negative E_x, positive B_y arises from reflections from the refractive index transition at the bottom of the resistive region. (*c*) $t = 1.2$. Wave energy returns from the highly conducting ionosphere, with $(B_y)_{max} = 23$ nT just above it (cell [22,76]) as expected. $(E_x)_{max} = 0.71$ mV m^{-1} at (21,56). Maximum dissipation and downward $E_z = 0.9$ mV m^{-1}, occurs at (19,60). Complex reflection features with B_y negative, E_x positive, from the top and bottom E_x negative, B_y positive of the turbulent region can be seen behind the trailing flank of the pulse. (*d*) $t = 1.4$. Ionospherically reflected components with enhanced J_z pass back through the turbulent region driving up further parallel electric fields $E_z = 0.7$ mV m^{-1} at [17,60] and increasing local dissipation. Reflections from the resistive region behind the trailing flank are clearly seen, in both, the Poynting flux $S_z \propto E_x B_y$ is upwards. S_z is of course downwards in the body of the pulse.

The behaviour of this simulated system is very dynamic and complex. For further clarification we show in figure 2 profiles of E_x and B_y at various points in the system. Figure 2 shows snapshot comparisons of B_y and E_x profiles made at $t = 0.8, 1.0, 1.2, 1.4$, above, within, and below the turbulent region. The normalization $B_y = B_y/B_0$, $E_x = cE_x/V_{A0}$ implies $B_y = E_x$ for plane parallel propagating waves.

Figure 2*a*, at $t = 0.8$, shows these profiles in the free propagation phase and demonstrates the effect of finite electron inertia ($k_\perp c/\omega_p$) on the pulse profile. In figure 2*b* at $t = 1.0$, the enhanced E_x and reduced B_y features resulting from reflections from the resistive zone are clear (see (ii)), whereas in frame (iii) the B_y profile has undergone marked resistive diffusion. Freely downward propagating waves with the broadened field profiles are seen below the zone in frame (iv).

The final frames (*c*) are recorded at $t = 1.4$. Even in (i) at $z = 0.5L_z$ the effects of 'topside' reflections can be seen, while just above and within the resistive region (frames (ii), (iii)) reflections from both ionosphere and resistivity, together with resistive broadening contribute to the complexity of the profiles. The E_x/B_y ratio varies rapidly in both magnitude and sign, a crude indicator of Poynting flux variations. The relatively small E-field scale sizes are noteworthy and are the results of interference, mainly with upcoming components reflected from the ionosphere.

In sampling plane (v) between the ionosphere and turbulent zone the ratio of E/B is small, a consequence the E-field reversal on reflection at the lower boundary.

The general evolution of the current density can be inferred in figure 3, the profiles being recorded at $t = 1.4$.

Here, the profiles marked with open circles show $J_z(x)$ at the same z values as used in figure 2, with the $J_z(x)$ profile of frame (i) being included (solid line) for ease of comparison. Conventional current is positive upwards in the plots.

The current density $J_z = \pm 10\ \mu\text{A m}^{-2}$ prescribed at the generator is full vertical scale in these plots and, because initially $(J_z/J_c)_{max} = 5$, the frames illustrate both the diffusive reduction of this ratio to a value of about 2 within the turbulent zone, and also its subsequent enhancement in the ionospheric reflection phase.

An interesting quantity monitored by these simulations is the value of the integrated parallel electric field through the dissipative region. The E-field structures there are by no means curl free, but we note that at $t = 1.4$ (i.e. after two passes through the region) this quantity

$$\phi_z = -\int_{(\Delta z)_{turb}} E_z(x)\,\mathrm{d}z$$

has a maximum value of *ca.* 1.1 kV at $x = 30$ and *ca.* -950 V at $x = 20$, the slight asymmetry being due to the interference and generator motion. This is very large compared to the internal $\phi_z \approx \pm 80$ V in the earlier, free propagation phase. It is instructive to compare these values with that of $\int E_x\,\mathrm{d}x$ at the generator, $\phi_x \approx 3.3$ kV.

Figure 4 summarizes wave energy flow and dissipation at $t = 1.5$.

We have presented the results of a single run of this simulation code. It is important to point out that the code has been tested for wide variations of the input parameters, including those involving the generator itself, such as the perturbation ratio B_y/B_0 and the initial parallel current density J_z, by the choice of the value of $k_\perp c/\omega_p$. Parameters related to the resistive region, such as the nonlinear resistivity coefficients ν_1 and ν_2, the J_z/J_c ratio involving implied

PHILOSOPHICAL TRANSACTIONS OF THE ROYAL SOCIETY A MATHEMATICAL, PHYSICAL & ENGINEERING SCIENCES

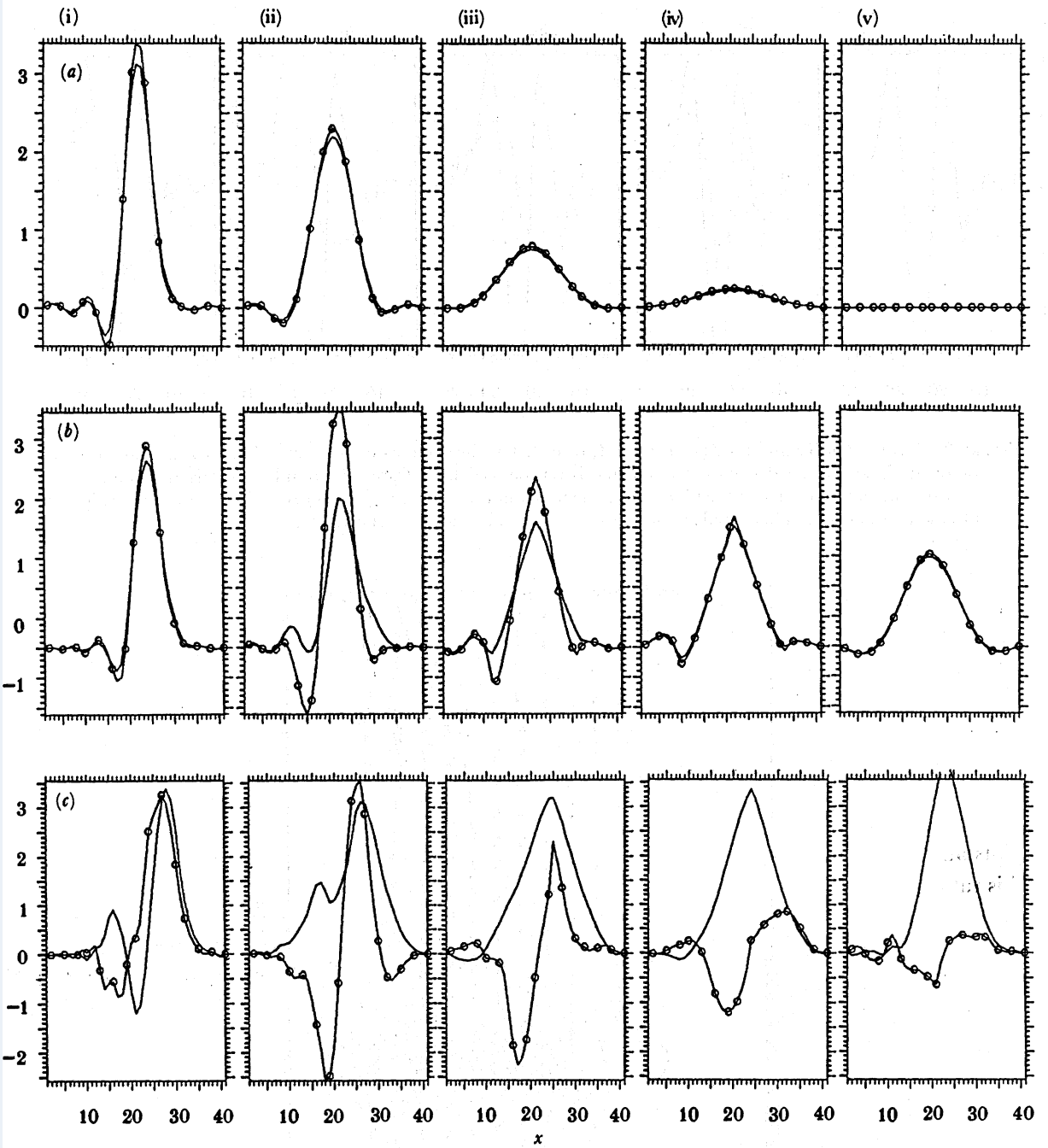

FIGURE 2. $(c/V_{A0})\,E_x(x)$ (open circles), $B_y(x)$ profiles at various z values above ((i) $z = \frac{1}{2}L_z = 40$ cells, (ii) $z = 54$), within ((iii) $z = 63$, (iv) $z = 66$), and below ((v) $z = 72$) the turbulent region. The scaling of E_x is such that for pure $(k_\perp c/\omega_p = 0)$ propagation the E_x and B_y profile would coincide. Vertical scales for B_y, 3 nT, and E_x, 90 mV m^{-1} per major scale division. (*a*) $t = 0.8$. Free propagation of shear wave, showing finite $k_\perp$ effects $|E_x| > |B_y|$ in the centre and wings of the pulse. S_z can be estimated roughly from $E_x B_y$ and is positive downward. (*b*) $t = 1.0$. In (ii) the effects of reflection; above the turbulent zone are seen in the E_x/B_y enhancements, and in (iii), (iv) the dissipative diffusion of the B_y profile. (*c*) $t = 1.4$. A variety of complex features related to reflections from the turbulence and ionosphere (see also figure 1 and text) together with the strong enhancement B_y just above the ionosphere as a result of wave reflection.

PHILOSOPHICAL TRANSACTIONS OF THE ROYAL SOCIETY A MATHEMATICAL, PHYSICAL & ENGINEERING SCIENCES

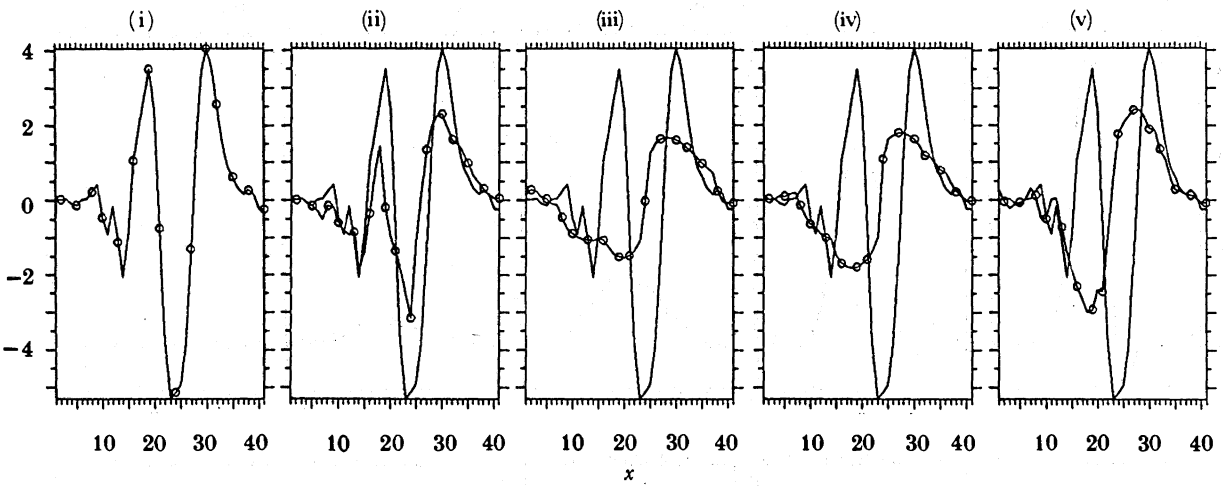

FIGURE 3. Current density profiles $J_z(x)$ at $t = 1.4$, recorded at the same values (i)–(v) as in figure 2. Those marked by open circles are local values, the full line is reproduced from frame (i) to aid comparison. Conventional upward current is positive in the plots where the maximum vertical range is 10 μA m^{-2}. The effect of dissipative broadening and ionospheric reflection can be seen in (iii) and (v) respectively.

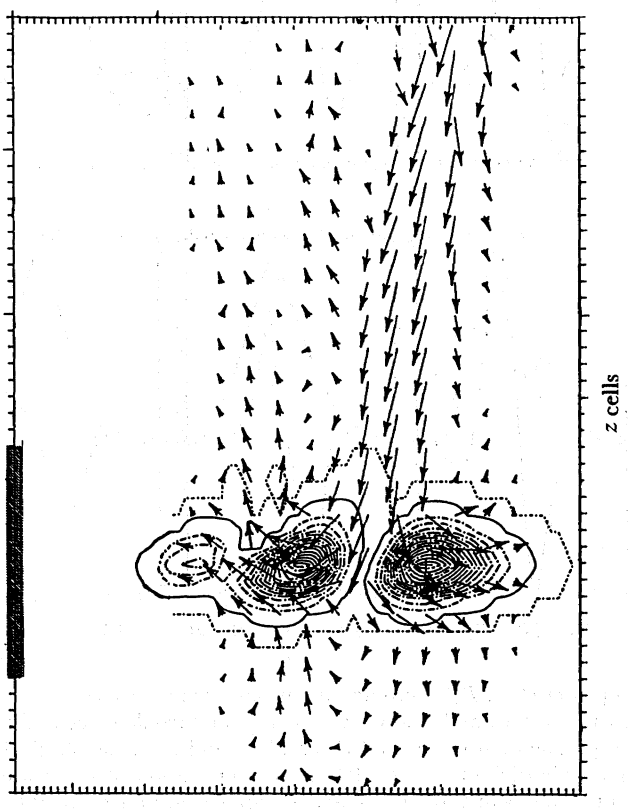

FIGURE 4. Wave energy flux $\boldsymbol{S}$ (vectors), and dissipation contours recorded at $t = 1.5$. The horizontal component of $\boldsymbol{S}$ is magnified to clarify flows in the vicinity of the resistive regions.

PHILOSOPHICAL TRANSACTIONS OF THE ROYAL SOCIETY A MATHEMATICAL, PHYSICAL & ENGINEERING SCIENCES

variation of the ion-to-electron temperature ratio, density and critical electron drift velocity (see L.D. Appendix A), and the actual spatial extent in z of the region were also varied systematically. The effects of magnitude and spatial modulation of the ionospheric height-integrated conductivity and of large-scale (in x) bias currents have also been studied.

The results of this wider study allow us to state rather generally that

(a) the complex and dynamic behaviour described here is typical of systems in which the field-aligned current exceeds the threshold for the onset of resistive effects (even including a resistivity law appropriate to saturated ion sound turbulence as discussed by Dum (1978)).

(b) the shear wave current-driven resistivity mechanism is a rather efficient generator of parallel electric fields and by implication, of accelerated electrons. If we take as a measure of performance the ratio of the integrated parallel electric field through the turbulent region to the integrated perpendicular electric field at the generator this ratio generally exceeds 0.3.

The 'robustness' of this result, with respect to details of the resistivity law invoked is due to the fact that if, for example, the current system is only weakly above the critical threshold in the first pass through the resistive zone it will be enhanced at the ionosphere to strongly supercritical values for the return passage. Conversely, an initially strongly supercritical current system will generate more intense parallel fields during its initial passage down through the resistive zone.

Observational aspects

The results underline the highly dynamic, rather electromagnetic, spatially dependent nature of Alfvén wave propagation in the presence of wave-induced turbulent resistivity, and raise a number of points that are of relevance in the interpretation of recent spacecraft data (see also Haerendel 1984; Falthammer 1985).

The *S*3-3 results (see the review by Mozer *et al.* (1980)) provide many seminal observations including the presence of ion cyclotron turbulence and double layers and the existence of strong (greater than 100 mV m^{-1}) short perpendicular-scale electric fields on auroral field lines. It was not possible to measure plausible magnetic components of these 'electrostatic' shocks, and similar structures, the pair of back-to-back 'S-shocks' in the simulation, remain rather electromagnetic on the relatively short timescales considered.

Recently explicit searches for Alfvén wave activity have been carried out by Dobrynin *et al.* (1984, 1986), Gurnett *et al.* (1984) and Berthelier *et al.* (1988).

The measurements demonstrate polarization in the plane perpendicular to B_0 with Berthelier *et al.* quoting examples of linear polarization with E–W oriented magnetic perturbations. The authors have stressed measurements of the E/B ratio in frequency ranges below the local O^+ gyrofrequency for the auroral zone and also the cusp (Berthelier *et al.*) flux tubes. Gurnett *et al.* conclude that the field ratio is consistent with Alfvén wave propagation and (reverting to SI units) with the ratio $\mu_0 E/B \approx V_A$ where V_A is calculated using estimates of the local plasma parameters, and with a small (net) downward Poynting flux. There is also considerable scatter in the field ratio at any given height (D. A. Gurnett, personal communication). Berthelier *et al.* find the expected altitude variation, but cite cases in which $\mu_0 E/B \gg V_A$, and note that regions containing large perturbations are associated with electron precipitation.

From the model viewpoint, a satellite passing through an Alfvén structure will experience a

PHILOSOPHICAL TRANSACTIONS OF THE ROYAL SOCIETY A MATHEMATICAL, PHYSICAL & ENGINEERING SCIENCES

mixture of time-dependent and space-dependent effects as can readily be seen in figure 2. Very generally one could say that the field ratio should be greater than V_A above a turbulent region, less than V_A within one and should approach the ionospheric value $\mu_0 E/B = (\Sigma_P)^{-1}$ at the lowest altitudes, but very considerable variations can be expected, particularly at frequencies where the satellite or convective doppler shift implies small scales. The anomalously high ratios recorded by Berthelier *et al.* are none the less mysterious.

In the absence of electric field measurements, high-resolution magnetometers can be used to estimate the magnitude of the field-aligned current density if one takes the view that the relative spacecraft-current sheet motion allows one to make an estimate of a component of $\nabla \times \boldsymbol{B}$ (in the model $\partial B_y/\partial x$).

On large spatial scales this current density is low, (Iijima & Potemera 1976), only a few microamps per square metre at 1000 km altitude, but a number of reports of very high current densities, in the tens to hundreds of microamps per square metre, exist on short (less than 1 to 10 km) spatial scales at heights of *ca.* 1000 km on auroral field lines (Sugiura *et al.* 1982; Burke *et al.* 1982, 1984; Bythrow *et al.* 1984; Berthelier *et al.* (1982, 1988). The observations point up a problem which has long troubled experimenters using rocket-borne particle experiments, that of identifying the current carriers and accounting for the magnitude of the current itself.

A much invoked interpretation is that, at least on inverted V-scales (*ca.* 50–100 km), the upward current carriers are electrons extracted from a trapped reservoir of hot magnetospheric electrons by a field-aligned potential drop (Knight 1973; Lemaire & Scherer 1974; Chiu *et al.* 1981; Lyons 1981). It can easily be seen (see, for example, Burke *et al.* 1982; Burke 1984) that, for reasonable plasma parameters, such a mechanism cannot account for $J_\parallel$ values much greater than a few microamps per square metre, nor for the small perpendicular-scale sizes observed. Results based on measurements of precipitating suprathermal electrons confirm this.

Compared with the new measurements the unexplained current component is thus very substantial, and in our view resides in the (unmeasured) thermal background electron component, the primary current carriers for an Alfvén wave.

We would also point out that current tubes or sheets of comparable mapped intensities have been identified in *Geos* II substorm-onset data at $6.6R_E$ ($R_E = 6.37 \times 10^6$ m) by Robert *et al.* (1984). The detailed way in which the self-consistent parallel current is carried in these more distant finite β regions is not known. The local plasma is rather mixed, with hot plasma sheet components ($n \approx 10^6$ m^{-3}, T_e (hot) $\approx$ keV) and cooler components of ionospheric origin, and implies large numbers of resonant electrons. The velocity space evolution of the current carriers during wave propagation down a flux tube on which mirror forces act together with effects of temperature, composition and density changes is obviously very complicated. The observations nevertheless strongly imply that auroral zone flux tubes carry wave-associated currents from distant nightside generating regions (e.g. pressure gradients and moving plasma associated with tail reconnection (Sato *et al.* 1982; Roux 1985 and his coworkers)). Along the same lines we would also surmise that the intense dayside current events (Burke *et al.* 1982; Sugiura *et al.* 1982) are associated with similar phenomena in frontside reconnection, or in flux transfer, generating regions. It is worth recalling that the perpendicular-scale size in such generating regions is of the order of the ion larmor radius which when mapped to the ionosphere is of the order of a few kilometres or less. For current densities of *ca.* 100 μA m^{-2} at 1000 km (*ca.* 10 μA m^{-2} at 6000 km) turbulent processes can be expected to occur locally,

PHILOSOPHICAL TRANSACTIONS OF THE ROYAL SOCIETY A MATHEMATICAL, PHYSICAL & ENGINEERING SCIENCES

because for $n_e \approx 10^9$ m^{-3}, the background drift velocity $V_d \approx 10^6$ m s^{-1}. Though the current is most unlikely to be carried by a simple drifting maxwellian distribution, turbulence is extremely likely to occur in the ICH-mode (and possibly ion sound) (Kindel & Kennel 1971), since a value of $V_d \approx 10^6$ m s^{-1} exceeds the linear ICH unstability threshold for a 1 eV O^+-dominated plasma by a factor of 10 or so.

Moreover, allowing for density and composition changes at heights above 1000 km, and including a $J_\parallel \propto B_0$ scaling, such instabilities are likely to be present sporadically over a rather extended region along the field line for lower currents at 1000 km level.

Relating observations of wave instabilities on auroral field lines to the turbulent dissipation required by the present model is not straightforward. There is no shortage of such observations (Gurnett & Frank 1977; Kintner *et al.* 1979; Mozer *et al.* 1980; André *et al.* 1987; Hultqvist *et al.* 1988), but their connection with supercritical electron drifts is by no means established. Many of the wave events have been associated with ion beam or ion conic distributions, which may themselves be linked with current-driven turbulence, and as noted earlier the measurement of drifting thermal electrons is a particularly difficult one. Moreover, although the wave turbulence (we include weak double layers (Mozer 1981)) may exist over extended regions it is likely to be very sporadic both in space and time and in part masked by strong quasi-direct-current electric fields.

At this stage we can only reiterate that a major feature of this model is its insensitivity to details of the anomalous resistivity law.

The current sheets modelled here have densities $J_z \approx \pm 10$ μA m^{-2} at 6000 km altitude, mapping to *ca.* 70 μA m^{-2} at 1000 km altitude. While the magnetic perturbations associated with them are small, $B_y/B_0 \approx 0.3\,\%$, the Poynting flux, if they were freely propagating Alfvén waves, S_z (6000 km) $\approx (\boldsymbol{E}\times\boldsymbol{B})/\mu_0 \approx 10^{-2}$ W m^{-2} is not trivial in terms of auroral energetics. Assuming, conservatively, that about 10 % of the incoming energy is channelled by dissipation into particle acceleration and heating, it is sufficient to produce *ca.* 5×10^{-2} W m^{-2} of precipitating particles at 1000 km. This compares rather favourably with typical energy fluxes of precipitating electrons over bright arcs of between 10^{-2} and 10^{-1} W m^{-2} sr^{-1}.

Energetics apart, further discussion of details of the acceleration process is outside the compass of this paper (see, for example, Falthammer 1985 for a review).

The model presented here stresses the role of small-scale structuring in magnetosphere–ionosphere coupling. The aurora, as seen from the ground with good angular resolution, is a beautiful manifestation of this with its interlacing of sheets and filaments and as stressed by Haerendel (1984) of complementary 'black forms'. The dissipative Alfvén model, with its paired up–down acceleration regions provides naturally for such phenomena and also for the observations of upwardly accelerated electrons on *ATS*-6 by McIlwain (1975) and more recently by Sharp *et al.* (1980) and Hultqvist *et al.* (1988).

It will be fascinating to see in future measurements of higher sensitivity to what extent the auroral zone flux tubes are permeated by such small-scale current systems.

It is a pleasure to acknowledge stimulating discussions with R. L. Lysak, G. Haerendel and R. A. Treumann and to thank the Max Planck Society who generously provided support to one of us (P.J.C.) during the course of the study.

References

Arykov, A. A. & Maltsev, Y. P. 1983 Generation of Alfvén waves in an anomalous resistivity region. *Planet. Space Sci.* **31**, 267.

Berthelier, J. J., Lefeuvre, F., Mogilevsky, M. M., Molchanov, O. A., Galperin, Y. I., Karczewski, J. F., Ney, R., Gogly, G., Guerin, C., Leveque, M., Moreau, J.-M. & Sene, F. X. 1982 Measurements of the VLF electric and magnetic components and DC electric field on board the *AUREOL*-3 spacecraft: the TEF-ONCH experiment. *Annls Geophysicae* **38**, 643.

Berthelier, J. J., Machard, C., Cerisier, J.-C., Berthelier, A. & Bosqued, J. M. 1988 ULF electromagnetic turbulence in the high-latitude topside ionosphere. *J. geophys. Res.* **93**, 5701.

Burke, W. J., Silevitch, M. & Hardy, D. A. 1983 Observations of small-scale vortices by the *S*3-2 satellite. *J. geophys. Res.* **88**, 3127.

Burke, W. J. 1984 Correction to 'Observation of small-scale auroral vortices by the *S*3-2 satellite' (Burke *et al.*) *J. geophys. Res.* **89**, 403.

Bythrow, P. F., Potemra, T. A., Hanson, W. B., Zanetti, L. J., Meng, C. I., Hoffman, R. E., Rich, F. J. & Hardy, D. A. 1984 Earthward directed high density Birkeland currents observed by HILAT. *J. geophys. Res.* **89**, 914.

Cerisier, J.-C., Machard, C. & Pottelette, R. 1987 MHD turbulence generated by time-varying field-aligned currents. *J. geophys. Res.* **92**, 11225.

Chui, Y. T. & Schultz, M. 1978 Self-consistent particle and parallel electrostatic field distributions in the magnetospheric–ionospheric auroral region. *J. geophys. Res.* **83**, 629.

Dubinin, E. M., Izrailevich, P. L., Nikolaeva, N. S. & Podgorny, I. M. 1986 The relationship between the electric and the magnetic field in the auroral MHD disturbances at altitude 1000 km. *Rep. Space Res. Inst.* Moscow: U.S.S.R. Academy of Science.

Dubinin, E. M., Izrailevich, P. L., Nikolaeva, N. S., Podgorny, I. M., Bankov, N. & Todorieva, L. 1985 Electromagnetic structures in the auroral latitudes (Intercosmos–Bulgaria–1300 satellite data). *Rep. Space Res. Inst.* Moscow: U.S.S.R. Adcademy of Sciences.

Dum, C. T. 1978 Anomalous heating by ion sound turbulence. *Phys. Fluids* **21**, 945.

Dum, C. T. 1981 Anomalous resistivity and plasma dynamics. In *Physics of auroral arc formation. Geophys. Monograph Series* no. 25, (ed. S.-I. Akasofu & J. R. Kan), p. 408. Washington, D.C.: American Geophysical Union.

Dum, C. T. 1985 Anomalous transport induced by field-aligned currents, and its relation to electromagnetic coupling. In *Unstable Current System and Plasma Instabilities in Astrophysics.* (ed. M. R. Kundu & E. D. Holman), p. 329.

Dum, C. T. & Dupree, T. H. 1970 Nonlinear stabilization of high-frequency instabilities. *Phys. Fluids* **13**, 2064.

Fridman, M. & Lemaire, J. 1980 Relationship between auroral electron fluxes and field-aligned electric potential difference. *J. geophys. Res.* **85**, 664.

Falthammer, C.-G. 1985 Magnetosphere–ionosphere coupling. *ESA* **SP-235**, 107.

Goertz, C. K. & Boswell, R. W. 1979 Magnetosphere–ionosphere coupling. *J. geophys. Res.* **84**, 7239.

Goertz, C. K. 1981 Discrete break-up arcs and kinetic Alfvén waves. In *Physics of the auroral arc formation. Geophys. Monograph Series*, no. 25, p. 451. Washington, D.C.: American Geophysical Union.

Gurnett, D. A., Huff, R. L., Menietti, J. D., Burch, J. L., Winningham, J. D. & Shawhan, S. D. 1984 Correlated low-frequency electric and magnetic noise along auroral field lines. *J. geophys. Res.* **89**, 8971.

Gurnett, D. A. & Frank, L. A. 1977 A region of intense plasma wave turbulence on auroral field lines. *J. geophys. Res.* **82**, 1031.

Haerendel, G. 1983 An Alfvén model of auroral arcs. In *High-latitude space plasma physics* (ed. B. Hultquist & T. Hagfors), p. 515. New York: Plenum.

Hasegawa, A. 1976 Particle acceleration by MHD surface wave and formation of aurora. *J. geophys. Res.* **91**, 5083.

Hultqvist, B., Lundin, R., Slasewicz, K., Block, L., Lundquist, P. A., Gustaffson, G., Koskinen, H., Bahnsen, A., Potemra, T. A. & Zanetti, L. J. 1988 Simultaneous observations of upward moving field-aligned energetic electrons and ions on auroral zone field lines. *J. geophys. Res.* **93**, 9765.

Iijima, I. & Potemra, T. A. 1978 Large-scale characteristics of field-aligned currents associated with substorms. *J. geophys. Res.* **83**, 599.

Kan, J. R. 1982 Towards a unified theory of discrete auroras. *Space Sci. Rev.* **31**, 71.

Kindel, J. M. & Kennel, C. F. 1971 Topside current instabilities. *J. geophys. Res.* **76**, 3055.

Kintner, P. M., Kelley, M. C., Sharp, R. D., Ghielmetti, G., Temerin, M., Cattell, C. A., Mizera, P. F. & Fennel, J. F. 1979 Simultaneous observations of energetic (keV) ions and electrostatic hydrogen cyclotron waves. *J. geophys. Res.* **84**, 7201.

Knight, S. 1973 Parallel electric fields. *Planet. Space Sci.* **21**, 741.

Lemaire, J. & Scherer, M. 1974 Ionosphere–plasmasheet field-aligned currents and parallel electric fields. *Planet. Space Sci.* **22**, 1485.

Lyons, L. R. 1980 Generation of large-scale regions of auroral precipitation, electric potentials and precipitation by the divergence of the convection electric field. *J. geophys. Res.* **85**, 17.

PHILOSOPHICAL TRANSACTIONS OF THE ROYAL SOCIETY A MATHEMATICAL, PHYSICAL & ENGINEERING SCIENCES

Lysak, R. L. 1985 Auroral electrodynamics with current and voltage generators. *J. geophys. Res.* **90**, 4178.
Lysak, R. L. & Carlson, C. W. 1981 The effect of microscopic turbulence on 1400. *Geophys. Res. Lett.* **8**, 269.
Lysak, R. L. & Dum, C. T. 1983 Dynamics of magnetosphere–ionosphere coupling including turbulent transport. *J. geophys. Res.* **88**, 365.
Lysak, R. L. & Hudson, M. K. 1979 Coherent anomalous resistivity in the region of electrostatic shocks. *Geophys. Res. Lett.* **6**, 661.
Mallinckrodt, A. J. & Carlson, C. W. 1978 Relations between transverse electric fields and field-aligned currents. *J. geophys. Res.* **83**, 1426.
Maltsev, Y. P., Lyatsky, W. B. & Lyatskya, A. M. 1977 Currents over the auroral arc. *Planet. Space Sci.* **25**, 53.
McIlwain, C. E. 1975 Auroral electron beams near the geomagnetic equator. In *Nobel Symp. Proc.* New York: Plenum.
Mozer, F. S. 1981 Observations of double layers on auroral field lines between 2.5 and 7 earth radii. *Geophys. Res. Lett.* **8**, 832.
Mozer, F. S., Carlson, C. W., Hudson, M. K., Torbert, R. B., Yatteau, J. & Kelley, M. C. 1977 Observations of paired electrostatic shocks in the polar magnetosphere. *Phys. Rev. Lett.* **38**, 292.
Mozer, F. S., Cattell, C. A., Hudson, M. K., Lysak, R. L., Temerin, M. & Torbert, R. B. 1980 Satellite measurements and theories of auroral acceleration. *Space Sci. Rev.* **27**, 155.
Nishida, A. 1979 Possible origin of transient dawn-to-dusk electric field in the nightside magnetosphere. *J. geophys. Res.* **84**, 3409.
Persoon, A. M., Gurnett, D. A. & Shawhan, S. D. 1983 Polar cap electron densities from *DE*1 plasma wave observations. *J. Geophys. Res.* **88**, 10, 123.
Robert, P., Gendrin, R., Perrault, S., Roux, A. & Pedersen, A. 1984 *GEOS*-2 identification of rapidly moving current structures in the equatorial outer magnetosphere. *J. geophys. Res.* **89**, 819.
Roux, A. 1985 Generation of field-aligned structures at substorm onset. *ESA* **SP-235**, 151.
Sato, T. 1978 A theory of quiet auroral arcs. *J. geophys. Res.* **83**, 1042.
Sato, T. & Ijima, T. 1979 Primary sources of large-scale Birkeland currents. *Space Sci. Rev.* **24**, 347.
Scholer, M. 1970 On the motion of artificial ion clouds in the magnetosphere. *Planet. Space Sci.* **18**, 977.
Sharp, E. G., Shelley, E. G., Johnson, R. G. & Ghielmetti, A. G. 1980 Counterstreaming electron beams of altitudes of *ca.* $1R_E$ over the auroral zone. *J. geophys. Res.* **85**, 92.
Sugiura, M., Maynard, N. C., Farthing, W. H., Heppner, J. P., Ledley, B. G. & Cahill, L. J. 1982 Initial results on the correlation between the electric and magnetic fields observed from the DE-2 satellite in the field-aligned current regions. *Geophys. Res. Lett.* **9**, 985.

PHILOSOPHICAL TRANSACTIONS OF THE ROYAL SOCIETY A MATHEMATICAL, PHYSICAL & ENGINEERING SCIENCES